Published in final edited form as:
Semin Radiat Oncol. 2014 July ; 24(3): 210–217. doi:10.1016/j.semradonc.2014.02.002.

MRI of the tumor microenvironment in radiotherapy: perfusion, hypoxia and metabolism

Masayuki Matsuo[1], **Shingo Matsumoto**[1], **James B. Mitchell**[1], **Murali C. Krishna**[1], and **Kevin Camphausen**[2]

[1]Radiation Biology, Center for Cancer Research, National Cancer Institute, National Institutes of Health, Bethesda, MD, USA

[2]Radiation Oncology Branches, Center for Cancer Research, National Cancer Institute, National Institutes of Health, Bethesda, MD, USA

Abstract

The tumor microenvironment is characterized by hypoxia, low pH, and high interstitial fluid pressure. Hypoxic regions in tumors with low pO_2 levels can result in resistance to radiotherapy causing local failure. It would therefore be desirable to non-invasively measure pO_2 levels in the tumor prior to, during, and after treatment to better customize therapy and follow treatment response. Several techniques used in pre-clinical and clinical studies to obtain pO_2 status of tissue such as dynamic contrast enhanced MRI (DCE-MRI), blood oxygen level dependent imaging (BOLD-MRI), and Electron Paramagnetic Resonance Imaging (EPRI) are reviewed. Furthermore, the ability to hyperpolarize specific metabolic substrates isotopically labeled with ^{13}C coupled with magnetic resonance spectroscopy enables non-invasive imaging of tissue metabolism such as glycolysis..

Introduction

Low partial pressure of oxygen (pO_2) tissue levels are linked to many pathophysiological conditions (e.g., ischemic diseases, reperfusion injury, and resistance to some forms of cancer treatment). At pO_2 levels < 10 mm Hg tumor cells and solid tumors in vivo become resistant to radiation treatment [1, 2] because oxygen is necessary to fix (enhance) radiation-induced damage to targets of ionizing radiation. Tumor hypoxia can be diffusion limited (chronic) or perfusion limited (acute) [3]. Many solid tumors outgrow the blood supply and, therefore, have some regions which display chronic and cycling hypoxia [4-7]. Hypoxia has been shown to exist in human tumors and is associated to resistance to radiotherapy [8]. Cancer cells harbored within these hypoxic regions survive the hypoxic tumor microenvironment by preserving limited amount of oxygen for more critical physiological pathways [9, 10] and generate energy by not only mitochondrial oxidative phosphorylation but also aerobic glycolysis. The characteristic high glycolytic activity is observed in wide

variety of tumors. Therefore, for comprehensive understanding of the accelerated glycolytic metabolism in individual tumors, both tumor oxygenation and energy metabolism need to be monitored simultaneously and non-invasively [11].

Imaging techniques which can provide maps of tumor pO_2 and metabolic profile can be valuable in guiding therapies, especially radiotherapy where images with information pertinent to physiology and/or metabolism can be integrated to radiation treatment planning [12] or combination therapies with a radio sensitizer, a hypoxia-specific cytotoxin or a hypoxia activated pro-drug [13]. In a recent review, the importance of integrating biological images to guide radiotherapy has been discussed [14, 15].

Here we review the current evidence supporting the use of MRI in this regard both in preclinical and clinical usage.

MRI

There are several techniques in use in preclinical and clinical studies to obtain pO_2 status of tissue [12]. Oxygen electrodes can provide quantitative assessment of tissue pO_2, but are invasive point measurements and are not amenable to deep-seated tumors. PET hypoxia imaging is non-invasive yet provides images which are qualitative in nature. Several other methods are in development of which Overhauser magnetic resonance imaging (OMRI), electron paramagnetic resonance imaging (EPRI) and ^{19}F MRI represent non-invasive and quantitative imaging approaches for mapping pO_2[16]. Additionally MRI techniques such as dynamic contrast-enhanced (DCE)–MRI, and blood oxygen level dependent (BOLD) provide information pertaining to local microenvironmental properties in the tumor such as perfusion, oxygenation, and cellular architecture.

DCE–MRI was found to correlate directly with oxygenation levels measured using the Eppendorf oxygen electrode in cervical cancer [17, 18]. Mayr *et al.* [19] demonstrated the prognostic value of assessing tumor enhancement, using gadolinium and dynamic MRI, in cervical carcinoma treated with radiation therapy. High levels of tumor enhancement before therapy or early in the course of therapy were associated with good local control. Furthermore, Yamashita *et al.* [20] showed histologically that in cervical tumors, poorly enhancing areas of dynamic MR images contain fewer capillaries and more abundant fibrous tissue. Both authors suggested that high levels of contrast enhancement might reflect better tumor oxygenation. DCE–MRI is not only to detect the tumor, but also the MR technique whose measurements have been correlated with radiotherapy outcome for patients with cervical tumors, concluding that patients with hypoxic tumors have a poorer response to radiotherapy in clinical treatment [21-23]. Recently Halle, C et al. [24] showed DCE-MRI visualized hypoxia and its molecular basis in chemoradioresistant tumors and they suggested the use of DCE-MRI to identify patients with treatment-resistant tumors that may benefit from additional or alternative therapy targeting hypoxia [25].

BOLD contrast is a functional MRI method that measures blood oxygenation using gradient echo sequences sensitive to changes in T2*. The method is based on the fact that deoxyhemoglobin is paramagnetic, whereas oxyhemoglobin is not. Therefore, changes in deoxyhemoglobin content in blood will influence water relaxation (particularly T2*),

enabling blood oxygenation levels to be indirectly monitored by MRI[26]. Hoskin et al. [27] showed that BOLD-MRI had high sensitivity but low specificity for defining intraprostatic tumor hypoxia; this together with the negative predictive value of 70% when combined with blood volume information makes BOLD-MRI a potential non-invasive technique for mapping prostatic tumor hypoxia. However, a quantitative relationship between the BOLD effect and pO_2 has not been found [28], probably because of the complex relationship between these two parameters [29]. Indeed, in addition to oxygenation, the BOLD effect is influenced by other factors, including blood flow, hemoglobin levels, vasculature, etc [26]. Molecular oxygen has two unpaired electrons and may act as a paramagnetic contrast agent, shortening the water T1 value, thus reflecting tissue oxygenation rather than blood oxygenation. Based on this, recently Hallac et al. [30] proposed a new methodology BOLD and tissue oxygen level dependent (TOLD) contrast MRI. Preliminary data suggest that these results provide further insight into the relationships between oxygen sensitive (BOLD/TOLD) MRI and tumor pO_2. These results agree well with previous reports using quantitative ^{19}F NMR oximetry [26].

Various approaches of MRS have been reported using ^{19}F labeled probes for NMR oximetry. Tumor oxygenation has also been monitored using oxygen sensitive MR reporter molecules (^{19}F-oximetry) [26]. However, this imaging agent needs to be injected directly into tumors, which clinically would limit its potential application[17].

EPRI

EPRI is a spectroscopic technique similar to nuclear magnetic resonance. EPR detects paramagnetic species that have unpaired electrons such as transition metal complexes and free radicals. Suitable agents for EPR imaging should have simple EPR spectra, and should be administered at levels which are well tolerated and should have pharmacological half-lives longer than the imaging time. OX063 is well suited as a paramagnetic agent in EPRI *in vivo*, to study tumor pO_2, dynamics of pO_2 to distinguish chronic versus acute hypoxia, and also monitor changes serially in response to therapy. Using triarylmethyl radical (TAM) such as OX063, EPRI is now being explored for mapping tissue oxygen in live animals [31-33]. EPRI represents a noninvasive, quantitative, and serial imaging approach for mapping pO_2 [34].

Though dissolved molecular oxygen is paramagnetic, it cannot be detected directly by EPR. The pO_2 imaging capability in EPR stems from the fact that the paramagnetic molecular oxygen affects the relaxation rates of the paramagnetic OX063 causing spectral broadening. The spectral broadening of OX063 is linearly proportional to the oxygen concentration. For imaging tumor pO2, an EPR imaging spectrometer operating at a frequency of 300 MHz (similar frequency as a 7 T MRI scanner) and a magnetic field of 10 mT was developed and the image formation and reconstruction approaches were integrated [31]. The quantitative pO_2 imaging in defined phantom objects and in *in vivo* models was validated in several studies [31]. Figure 1A (left) shows the anatomic image with the tumor bearing leg on the left. The image on the right in Figure 1A is a pO_2 map from the same mouse obtained from EPRI after infusion of OX063 (1.1 mmol/kg) when the mouse was breathing air. This tumor

displayed well-oxygenated regions and hypoxic regions. This experiment suggests the quantitative pO_2 imaging capability of EPRI.

Further developments in EPRI capabilities made it possible to obtain pO_2 maps in three dimensions in ~ 3 min making it possible to apply this technique to study spatio-temporal dynamics of pO_2 in tumors. To visualize dynamic changes of tumor oxygenation over a time period of 30 minutes, EPRI experiments were carried out collecting nine image data sets, each taking ~ 3 minutes, and three-dimensional reconstruction of pO_2 maps as well as the tracer distribution was conducted. Figure 1B shows the anatomic image of a SCCVII tumor obtained from MRI with four regions of interest (ROI) indicated. Figure 1C shows the corresponding time-dependent changes in pO_2 (top row) and the levels of TAM (bottom row) obtained by. The tumor oxygen levels displayed significant fluctuations, whereas the tracer level during this time window remained relatively stable. When tumor oxygen levels and TAM tracer levels in the four ROIs identified in the anatomic image (Fig. 1B) were plotted as a function of time, ROIs 1 and 2 displayed significant fluctuations in pO_2 (approximately 18-fold and 12-fold, respectively), whereas ROIs 3 and 4 displayed relatively smaller changes (~2-fold). No significant changes in the TAM tracer level were observed across the time course (Fig. 1D, right). Comparing the pO_2 maps and the tracer levels as a function of time (Fig. 1C and D), it can be seen in ROI 4 that though the tracer level was adequate enough for detection and imaging, yet this region displayed significant hypoxia. On the other hand, in the three remaining ROIs in which the tracer level was high and stable, the temporal fluctuations of pO_2 were significant, supporting previous observations of cycling hypoxia [6]. The data analyzed in this manner show that the time averaged pO_2 maps from EPRI can distinguish both chronically hypoxic and cycling hypoxic regions.

Using EPRI and MRI in tumor-bearing mice, we examined the vascular renormalization process by longitudinally mapping tumor partial pressure of oxygen (pO_2) and microvessel density during treatments with the multi-tyrosine kinase inhibitor sunitinib. Figure 2A (left) shows images of tumor pO_2 and microvessel density from SCC tumors treated with sunitinib 10 days after tumor implantation. The other images were taken on days 2 and 4 after initiating sunitinib treatment. Even in this tumor, which had significant hypoxic regions, tumor oxygen levels increased 2 and 4 days after sunitinib treatment compared with oxygen level before treatment (Fig. 2A, top). It should be noted that no significant change in tumor size occurred during these time points, despite a 45% reduction in tumor blood volume (Fig. 2A bottom). The transient increase in tumor pO_2 was quantified (Fig. 2B). As hypoxic cells show resistance to radiation, a transient increase in tumor oxygenation has a potential to improve treatment effect of radiation. A combination of 10 Gy radiation at the end of 4 days sunitinib treatment synergistically delayed the tumor growth (8 days) compared with radiation alone (2-day delay) or 4 days of sunitinib treatment (2-day delay, Fig. 2C). Collectively, microenvironmental changes resulting from normalization of tumor blood vessels by antiangiogenic treatment contributed to the improved efficacy of radiotherapy during the window of improved tumor oxygenation that can be directly monitored with EPRI. Radiation treatment during this time period of improved oxygenation by antiangiogenic therapy resulted in a synergistic delay in tumor growth. Sunitinib treatment suppressed the extent of temporal fluctuations in tumor pO_2 during the vascular

normalization window, resulting in the decrease of cycling tumor hypoxia [35]. In summary, EPRI is a promising non-invasive imaging modality that directly measures oxygen concentration in tumors in a 3D volume with spatial resolution of ~ mm and temporal resolution of minutes. The radiofrequency (300 MHz) power used provides the capability of imaging deep-seated tumors. Currently EPRI is a robust preclinical pO2 imaging technique capable of studying mice, rats, rabbits. With scale-up development to humans, EPRI has the capability to provide images of the tumor pO_2 and its dynamics, which can be used to deliver appropriate cancer treatment [16].

Hyperpolarized Metabolic MR

The signal to noise ratio in MRI depends on the polarization of the spin states, of nuclei such as ^{1}H, ^{13}C in addition to their nuclear magnetic moments, and the magnetic field strength of the MRI scanner. The polarization of ^{13}C at a magnetic field strength of 3 T is 2.5 parts per million. Thus, biological molecules enriched with ^{13}C suffer from poor sensitivity because of a lower magnetic moment, lower polarization and lower concentrations. The polarization of nuclei can be increased by different methods of which dynamic nuclear polarization (DNP) is the most successful [36, 37]. Since the chemical shifts of various organic molecules display significant differences, it is possible to inject a hyperpolarized ^{13}C labeled agent and follow its breakdown by chemical shift imaging or magnetic resonance spectroscopic imaging (MRSI). Pyruvate labeled with ^{13}C in the C-1 position is a molecule that satisfies all the conditions listed above and also is a key intermediate involved in major energy generating pathways in cells. Pyruvate is utilized to generate ATP through oxidative phosphorylation generating CO_2 as a byproduct, which is in equilibrium with HCO_3^- in a pH dependent manner with its unique chemical shifts. It is also converted to lactate through aerobic glycolysis or alanine through transamination.

Albers et al [38] have used a transgenic mouse model for prostate cancer and applied this method to determine the capability to distinguish malignancy and correlate with histology. In this study they show spectra from hyperpolarized [1-^{13}C] pyruvate injected in a mouse bearing a high grade tumor and the time course of the various products. These experiments show that the lactate signal reaches a maximum about 20 s after the pyruvate bolus arrival. The time course suggests that a time window between 30-60 s from start of injection is suitable for MRSI when the lactate levels were relatively constant. This study shows the feasibility of performing *in vivo* metabolic MRI with hyperpolarized ^{13}C labeled agents and that regions can be distinguished based on their metabolic profile and identifies a time window for imaging. They further implemented the imaging experiments in TRAMP (transgenic adenocarcinoma of mouse prostate) mice bearing a large primary tumor and a lymph node metastasis. Figure 3A shows anatomic image indicating the primary tumor and the lymph node metastasis and the corresponding image of pyruvate distribution (Figure 3B). A grid was placed on the tumor region (Figure 3C) from which the spectra in each voxel are displayed in Figure 3D. The spectra show high levels of lactate in the tumor and lymph node metastasis. Further studies in this report examined the relationship of the glycolytic activity monitored by MRI and histological exam of malignancy. Results from this study further support the relationship between the MRI data and histological experiments (Figure 3E). The normal prostate region displayed the lowest lactate/pyruvate

ratio whereas this ratio increased in histologically determined tumor grade. From this study, the correlation of the image data (lactate/pyruvate ratio) and the histologic assessment of the tumor grade validate this as an imaging biomarker for tumor grade.

Metabolic MRI with DNP has similar capabilities with additional advantages of rapid imaging, high SNR and no background. Monitoring the metabolic conversion of hyperpolarized pyruvate to lactate and using lactate/pyruvate as a biomarker can be a useful imaging biomarker for treatment response especially with support from the study of Albers et al., where a strong correlation between the malignancy and the lactate/pyruvate ratio was found.

The study of Day and our group tested this hypothesis of lactate/pyruvate as a biomarker for radiation therapy response using a glioma tumor model in rat treated to 15 Gy [39]. This research studied rats implanted with C6 glioma tumors studied with metabolic MRI using hyperpolarized [1-^{13}C]pyruvate and the lactate monitored with MRSI before treatment, and after treatment imaging was started 24 hr after irradiation, and the animals were followed longitudinally and reimaged at combinations of 48, 72 and 96 hr after treatment.

Figure 4 shows representative images of hyperpolarized ^{13}C pyruvate and lactate in a C6 glioma-bearing animal before (Figure 4B, C, D top) and 96 hr after radiotherapy (Figure 4B, C, D bottom). Comparison of spectra from tumor voxels with those on the contralateral side of the brain showed that the lactate signal was much higher in the tumor than in brain (Figure 4A). 13C chemical shift images acquired following intravenous injection of hyperpolarized [1-^{13}C]pyruvate into rats with implanted C6 gliomas showed significant labeling of lactate within the tumors but comparatively low levels in surrounding brain. Labeled pyruvate was observed at high levels in blood vessels above the brain and from other major vessels elsewhere but was detected at only low levels in tumor and brain. The ratio of hyperpolarized ^{13}C label in tumor lactate compared to the maximum pyruvate signal in the blood vessels was decreased from 0.38 to 0.23, (a reduction of 34%) by 72 h following whole brain irradiation with 15 Gy.

The first clinical trial of hyperpolarized [1-^{13}C]pyruvate metabolic imaging of prostate cancer patients was conducted at the University of California in San Francisco. This study was a proof-of-concept study entitled: A Phase 1/2a Ascending-Dose Study to Assess the Safety and Tolerability and Imaging Potential of Hyperpolarized Pyruvate (^{13}C) Injection in Subjects with Prostate Cancer. The secondary objective of this study was to determine the kinetics of hyperpolarized pyruvate delivery and metabolism throughout the prostate, and to determine the signal to noise ratio for pyruvate metabolites in regions of cancer and in surrounding benign prostate as a function of the dose of the hyperpolarized [1-^{13}C]pyruvate. All doses were well tolerated without exception, and excellent contrast-to-noise for [1-^{13}C] lactate was observed even at the lowest dose. Thus, hyperpolarized metabolic MR will be able to utilize multiple probes such as bicarbonate for pH, fumarate to monitor necrosis, ascorbate for redox status to follow specific metabolic processes in key biochemical pathways to obtain imaging biomarkers for radiation therapy response.

Conclusion

Hypoxia is a clinically relevant problem for radiotherapy and there are a number of potential imaging approaches that could be used to identify such hypoxic tumors [17]. Emerging pre-clinical and clinical imaging modalities are adding important physiological and metabolic dimensions to anatomic images. Such capabilities will provide valuable biological characterization of tumors in terms of non-invasive imaging biomarkers to design appropriate treatments based on tumor microenvironment. These imaging biomarkers will also be useful to monitor treatment response. Imaging pO_2 in tumors is now a robust pre-clinical imaging modality with potential for implementation clinically. Pre-clinical studies and the initial clinical study with hyperpolarized metabolic MR have been successful and may be part of image-guided radiotherapy to select patients for tailored individual treatment regimens.

This new approach of cancer imaging serves as non-invasive imaging biomarkers for studying tumor physiology and metabolism in preclinical and clinical research. We believe this combination has great potential for clinical applications for a new perspective in molecular imaging for radiation therapy.

Acknowledgments

This research was supported by the Intramural Research Program of the Center for Cancer Research, National Cancer Institute, NIH.

References

1. Horsman MR, Nordsmark M, Overgaard J. Techniques to assess the oxygenation of human tumors. State of the art. Strahlenther Onkol. 1998; 174(Suppl 4):2–5. [PubMed: 9879339]
2. Stratford IJ, Adams GE, Bremner JC. Manipulation and exploitation of the tumour environment for therapeutic benefit. Int J Radiat Biol. 1994; 65:85–94. [PubMed: 7905915]
3. Chaplin DJ, Olive PL, Durand RE. Intermittent blood flow in a murine tumor: radiobiological effects. Cancer Res. 1987; 47:597–601. [PubMed: 3791244]
4. Dewhirst MW. Relationships between cycling hypoxia, HIF-1, angiogenesis and oxidative stress. Radiat Res. 2009; 172:653–665. [PubMed: 19929412]
5. Matsumoto S, Yasui H, Mitchell JB. Imaging cycling tumor hypoxia. Cancer Res. 2010; 70:10019–10023. [PubMed: 21159626]
6. Yasui H, Matsumoto S, Devasahayam N. Low-field magnetic resonance imaging to visualize chronic and cycling hypoxia in tumor-bearing mice. Cancer Res. 2010; 70:6427–6436. [PubMed: 20647318]
7. Dewhirst MW. Intermittent hypoxia furthers the rationale for hypoxia-inducible factor-1 targeting. Cancer Res. 2007; 67:854–855. [PubMed: 17283112]
8. Thomlinson RH, Gray LH. The histological structure of some human lung cancers and the possible implications for radiotherapy. Br J Cancer. 1955; 9:539–549. [PubMed: 13304213]
9. Gatenby RA, Gillies RJ. Why do cancers have high aerobic glycolysis? Nat Rev Cancer. 2004; 4:891–899. [PubMed: 15516961]
10. Kim JW, Tchernyshyov I, Semenza GL. HIF-1-mediated expression of pyruvate dehydrogenase kinase: a metabolic switch required for cellular adaptation to hypoxia. Cell Metab. 2006; 3:177–185. [PubMed: 16517405]
11. Gillies RJ, Gatenby RA. Adaptive landscapes and emergent phenotypes: why do cancers have high glycolysis? J Bioenerg Biomembr. 2007; 39:251–257. [PubMed: 17624581]

12. Tatum JL, Kelloff GJ, Gillies RJ. Hypoxia: importance in tumor biology, noninvasive measurement by imaging, and value of its measurement in the management of cancer therapy. Int J Radiat Biol. 2006; 82:699–757. [PubMed: 17118889]
13. Brown JM, Wilson WR. Exploiting tumour hypoxia in cancer treatment. Nat Rev Cancer. 2004; 4:437–447. [PubMed: 15170446]
14. Grau C, Muren LP, Hoyer M. Image-guided adaptive radiotherapy - integration of biology and technology to improve clinical outcome. Acta Oncol. 2008; 47:1182–1185. [PubMed: 18654901]
15. Grau C, Olsen DR, Overgaard J. Biology-guided adaptive radiation therapy - presence or future? Acta Oncol. 2010; 49:884–887. [PubMed: 20831476]
16. Krishna MC, Matsumoto S, Saito K. Magnetic resonance imaging of tumor oxygenation and metabolic profile. Acta Oncol. 2013; 52:1248–1256. [PubMed: 23957619]
17. Horsman MR, Mortensen LS, Petersen JB. Imaging hypoxia to improve radiotherapy outcome. Nat Rev Clin Oncol. 2012; 9:674–687. [PubMed: 23149893]
18. Cooper RA, Carrington BM, Loncaster JA. Tumour oxygenation levels correlate with dynamic contrast-enhanced magnetic resonance imaging parameters in carcinoma of the cervix. Radiother Oncol. 2000; 57:53–59. [PubMed: 11033189]
19. Mayr NA, Yuh WT, Magnotta VA. Tumor perfusion studies using fast magnetic resonance imaging technique in advanced cervical cancer: a new noninvasive predictive assay. Int J Radiat Oncol Biol Phys. 1996; 36:623–633. [PubMed: 8948347]
20. Yamashita Y, Baba T, Baba Y. Dynamic contrast-enhanced MR imaging of uterine cervical cancer: pharmacokinetic analysis with histopathologic correlation and its importance in predicting the outcome of radiation therapy. Radiology. 2000; 216:803–809. [PubMed: 10966715]
21. Loncaster JA, Carrington BM, Sykes JR. Prediction of radiotherapy outcome using dynamic contrast enhanced MRI of carcinoma of the cervix. Int J Radiat Oncol Biol Phys. 2002; 54:759–767. [PubMed: 12377328]
22. Mayr NA, Wang JZ, Zhang D. Longitudinal changes in tumor perfusion pattern during the radiation therapy course and its clinical impact in cervical cancer. Int J Radiat Oncol Biol Phys. 2009; 77:502–508. [PubMed: 19775824]
23. Andersen EK, Hole KH, Lund KV. Dynamic contrast-enhanced MRI of cervical cancers: temporal percentile screening of contrast enhancement identifies parameters for prediction of chemoradioresistance. Int J Radiat Oncol Biol Phys. 2011; 82:e485–492. [PubMed: 22014954]
24. Halle C, Andersen E, Lando M. Hypoxia-induced gene expression in chemoradioresistant cervical cancer revealed by dynamic contrast-enhanced MRI. Cancer Res. 2012; 72:5285–5295. [PubMed: 22890239]
25. Zhao D, Jiang L, Hahn EW. Tumor physiologic response to combretastatin A4 phosphate assessed by MRI. Int J Radiat Oncol Biol Phys. 2005; 62:872–880. [PubMed: 15936572]
26. Pacheco-Torres J, Lopez-Larrubia P, Ballesteros P. Imaging tumor hypoxia by magnetic resonance methods. NMR Biomed. 2011; 24:1–16. [PubMed: 21259366]
27. Hoskin PJ, Carnell DM, Taylor NJ. Hypoxia in prostate cancer: correlation of BOLD-MRI with pimonidazole immunohistochemistry-initial observations. Int J Radiat Oncol Biol Phys. 2007; 68:1065–1071. [PubMed: 17637389]
28. Baudelet C, Gallez B. How does blood oxygen level-dependent (BOLD) contrast correlate with oxygen partial pressure (pO2) inside tumors? Magn Reson Med. 2002; 48:980–986. [PubMed: 12465107]
29. Jordan BF, Crokart N, Baudelet C. Complex relationship between changes in oxygenation status and changes in R*2: the case of insulin and NS-398, two inhibitors of oxygen consumption. Magn Reson Med. 2006; 56:637–643. [PubMed: 16897769]
30. Hallac RR, Zhou H, Pidikiti R. Correlations of noninvasive BOLD and TOLD MRI with pO and relevance to tumor radiation response. Magn Reson Med. 2013
31. Matsumoto S, Hyodo F, Subramanian S. Low-field paramagnetic resonance imaging of tumor oxygenation and glycolytic activity in mice. J Clin Invest. 2008; 118:1965–1973. [PubMed: 18431513]

32. Matsumoto K, Subramanian S, Devasahayam N. Electron paramagnetic resonance imaging of tumor hypoxia: enhanced spatial and temporal resolution for in vivo pO2 determination. Magn Reson Med. 2006; 55:1157–1163. [PubMed: 16596636]
33. Saito K, Matsumoto S, Yasui H. Longitudinal Imaging Studies of Tumor Microenvironment in Mice Treated with the mTOR Inhibitor Rapamycin. PLoS One. 2012; 7:e49456. [PubMed: 23185335]
34. Ardenkjaer-Larsen JH, Laursen I, Leunbach I. EPR and DNP properties of certain novel single electron contrast agents intended for oximetric imaging. J Magn Reson. 1998; 133:1–12. [PubMed: 9654463]
35. Matsumoto S, Batra S, Saito K. Antiangiogenic agent sunitinib transiently increases tumor oxygenation and suppresses cycling hypoxia. Cancer Res. 2011; 71:6350–6359. [PubMed: 21878530]
36. Ardenkjaer-Larsen JH, Fridlund B, Gram A. Increase in signal-to-noise ratio of > 10,000 times in liquid-state NMR. Proc Natl Acad Sci U S A. 2003; 100:10158–10163. [PubMed: 12930897]
37. Golman K, Ardenkjaer-Larsen JH, Petersson JS. Molecular imaging with endogenous substances. Proc Natl Acad Sci U S A. 2003; 100:10435–10439. [PubMed: 12930896]
38. Albers MJ, Bok R, Chen AP. Hyperpolarized 13C lactate, pyruvate, and alanine: noninvasive biomarkers for prostate cancer detection and grading. Cancer Res. 2008; 68:8607–8615. [PubMed: 18922937]
39. Day SE, Kettunen MI, Cherukuri MK. Detecting response of rat C6 glioma tumors to radiotherapy using hyperpolarized [1- 13C]pyruvate and 13C magnetic resonance spectroscopic imaging. Magn Reson Med. 2011; 65:557–563. [PubMed: 21264939]

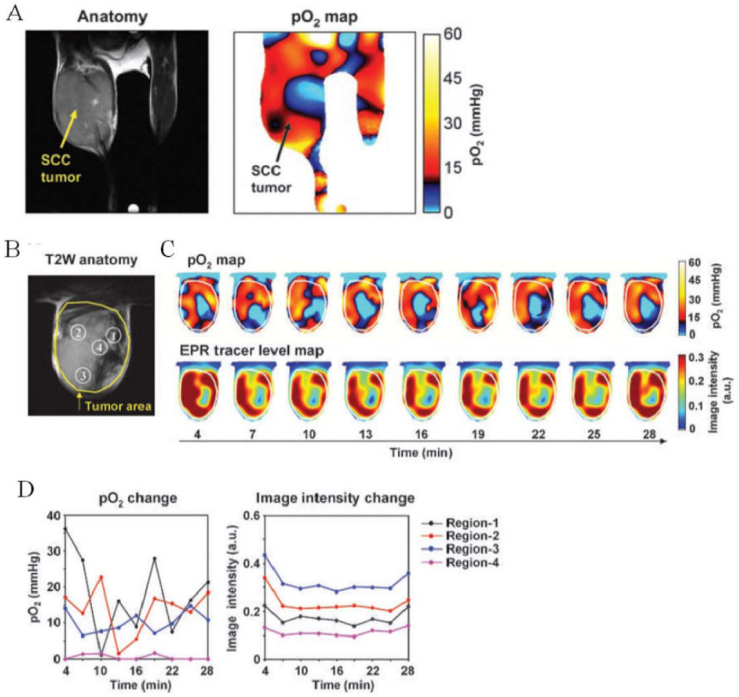

Figure 1.

A, EPR oxygen imaging of normal muscle in live mice. EPRI method allows the pO_2 map from deep in tissue of healthy mouse to be obtained. The anatomic image from MRI (left) of the lower body of a healthy mouse (without tumor bearing) and corresponding pO_2 map from EPRI (right) showed that the normal muscle region had relatively homogeneous pO_2 distribution.

B, T2-weighted anatomical image of a representative SCCVII tumor–bearing mouse. Large yellow line, tumor region. Four ROIs indicated by small white line were chosen for tracing fluctuations of pO_2 and spin intensity with time.

C, corresponding pO_2 maps (top) and the tracer level maps (bottom) were obtained from EPRI. Yellow line, tumor region. Time increased from left to right from 4 to 28 min.

D, the values of pO_2 and the tracer level in each ROI region, described in B, were quantified and plotted as a function of time.

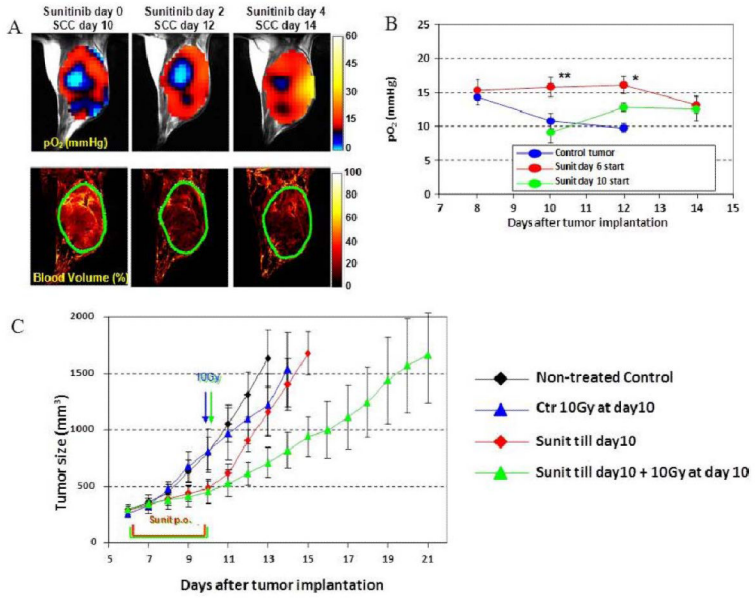

Figure 2.

Tumor pO_2 and blood volume imaging before and after antiangiogenic treatment initiated at the later stage of tumor.

A, initiation of antiangiogenic treatment at the later stage of tumor improved tumor oxygenation (top) and reduced tumor blood volume (bottom) without a significant change in tumor size.

B, Quantitation of pO_2 changes in sunitinib-treated and control mice. *, $P < 0.05$ **, $P < 0.01$.

C, Transient increase in tumor oxygenation by antiangiogenic treatment enhances outcome of radiotherapy. Tumor growth kinetic study was carried out on groups of tumor-bearing mice that include untreated control (black), single 10 Gy radiation at SCC day 10 (blue), 4 days sunitinib treatment during 6 to 10 days after SCC implantation (red), and 4 days sunitinib followed by single 10 Gy radiation (green).

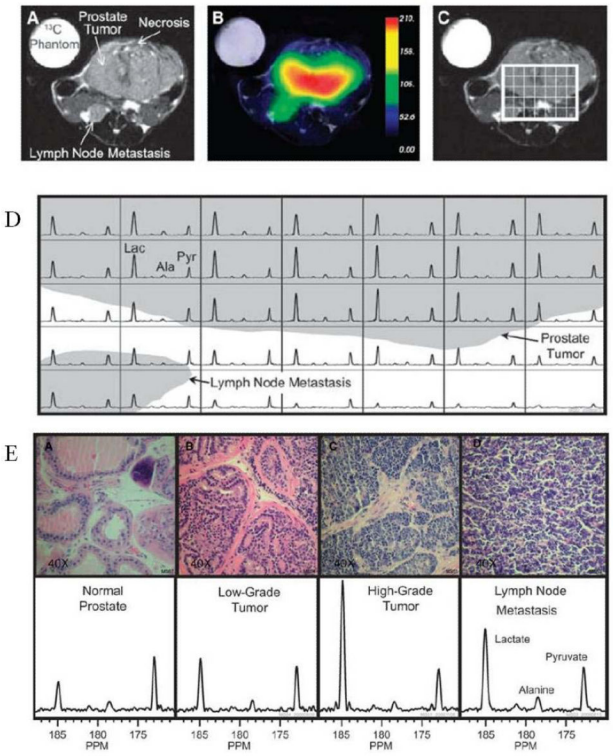

Figure 3.

Hyperpolarized ^{13}C metabolic images of a TRAMP mouse. Upper: The anatomonal image (A) and hyperpolarized ^{13}C lactate image (B) following the injection of hyperpolarized [1-^{13}C]pyruvate, overlaid on T_2-weighted ^{1}H image (C). Middle: Hyperpolarized ^{13}C spectra of primary and metastatic tumor regions (D). Lower: Representative H&E-stained sections and hyperpolarized ^{13}C spectra for one case from each of the histologically defined groups (E). The three-dimensional MRSI shows substantially elevated lactate in the high-grade primary tumor compared with the low-grade tumor. Lac, lactate; Ala, alanine; Pyr, pyruvate.

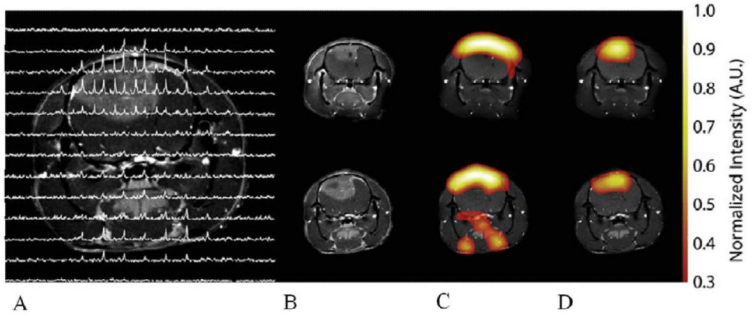

Figure 4.

Representative images of hyperpolarized 13C pyruvate (C) and lactate (D) in a C6 glioma-bearing animal before (top) and 96 h after radiotherapy (bottom). A CSI data set is shown in (A).The chemical shift images were superimposed on grayscale T1-weighted proton images (B) for anatomical reference. The lactate signals, in the false color images, were normalized to the maximum pyruvate signal in each dataset. The lactate signal was reduced following exposure to 15 Gy radiation.